ACS APPLIED MATERIALS & INTERFACES

Research Article

www.acsami.org

# Nanoscale Resistive Switching Schottky Contacts on Self-Assembled Pt Nanodots on $SrTiO_3$

Hyunsoo Lee,[†,‡] Haeri Kim,[§] Trong Nghia Van,[†,‡] Dong-Wook Kim,*[,§] and Jeong Young Park*[,†,‡]

[†]Center for Nanomaterials and Chemical Reactions, Institute for Basic Science, Daejeon 305-701, South Korea

[‡]Graduate School of EEWS and NanoCentury KI, KAIST, Daejeon 305-701, South Korea

[§]Department of Physics, Ewha Womans University, 52 Ewhayeodae-gil, Seodaemun-gu, Seoul 120-750, South Korea

**ABSTRACT:** A nanoscale Schottky diode using Pt nanodisks on a Nb-doped $SrTiO_3$ (Nb:STO) single crystal was fabricated, and resistive switching (RS) was demonstrated with conductive atomic force microscopy at ultrahigh vacuum. Pt disks with diameters on the order of 10 nm were formed using colloidal self-assembled patterns of silica nanospheres, followed by evaporation of the Pt layers on the Nb:STO single crystal. Here we show that the reproducible bipolar RS behavior of the nanoscale Pt/Nb:STO Schottky junction was achieved by utilizing local current−voltage spectroscopy. The conductance images, obtained simultaneously with topographic images, show the homogeneous current distribution of selected triangular-shaped Pt nanodisks during repetitive resistive switching between the high-resistance state (HRS) and low-resistance state (LRS). The endurance characteristics of the Pt/Nb:STO junction exhibit reliable switching behavior. These results suggest that the rectifying and resistive Pt/Nb:STO junction can be scaled down to the 10 nm range and their position can be controlled.

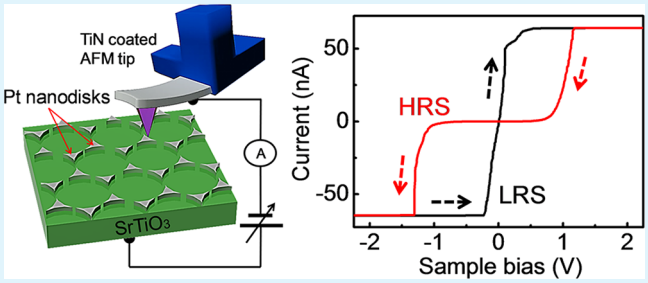


**KEYWORDS:** *Pt/Nb-doped $SrTiO_3$ single crystal, Schottky junction, scaling down, conductive atomic force microscopy, spatial mapping*

## 1. INTRODUCTION

The resistive switching (RS) phenomena induced by an electric field in metal oxides sandwiched between metal electrodes have continually attracted attention for next-generation, nonvolatile memory, so-called resistive random access memory (RRAM), due to their high-speed operation, low power consumption, and high storage density.[1−11] The rectifying Schottky-type diode is considered a strong candidate for inclusion in a device utilizing the crossbar array, a desirable architecture for ultimate-density RRAM.[12−14] In addition, investigation of the RS behaviors of the metal/oxide Schottky contact is very important for understanding the three major mechanisms of RS (e.g., formation/rupture of conducting filaments, the redox reaction effect, and the existence of charge-trapping states near the interface).[15]

Atomic force microscopy (AFM) has been used for electrical characterization of nanometer-scale RS phenomena due to its capability to measure local conductance.[16,17] In particular, AFM allows us to estimate the size of a conducting filament and investigate the spatial distribution of the switching sites.[12,18] Such results can provide insights regarding the capability to scale down RRAM devices. A few demonstrations of RS behavior using AFM with a metal-coated tip have been published. Alexe and co-workers demonstrated hysteretic switching in a nanoscale self-assembled $Bi_4Ti_3O_{12}$ ferroelectric memory cell via scanning force microscopy using piezoresponse mode.[19,20] Szot et al. observed the bistable switching behavior of undoped $SrTiO_3$ single crystals and attributed the RS origin to oxygen ion migration along the dislocations formed by Joule heating.[21] Nanoscale local RS behavior caused by individual filaments on $SrTiO_3$ thin films was also reported by utilizing local conductance AFM.[22,23] Migration of oxygen vacancies along structural defects and the electrochemical redox reaction are believed to play key roles in all of these results. Thus, the structural defect density[24] and spatial distribution of oxygen vacancies[25] will significantly influence the RS characteristics of a $SrTiO_3$ thin film. Such extrinsic factors will determine the switching sites, and RS cannot be achieved at a desired location. To guarantee scaling down of the RRAM devices, observation of nanoscopic RS phenomena alone is not enough; switching at a specific location should be enabled. In addition, the physical characteristics of an oxide thin film can be significantly affected by ambient conditions.[26] Surface adsorbates[27,28] and a pillar of water between the tip and surface of the sample, such as capillary condensation,[29] can hinder the current path and cause unwanted contamination. It is well-known that the near-surface electrochemical redox reaction is important in the RS mechanism. Therefore, RS characterization of the bare sample surface in air is very susceptible to extrinsic artifacts.

**Received:** August 2, 2013
**Accepted:** October 23, 2013
**Published:** October 23, 2013

  

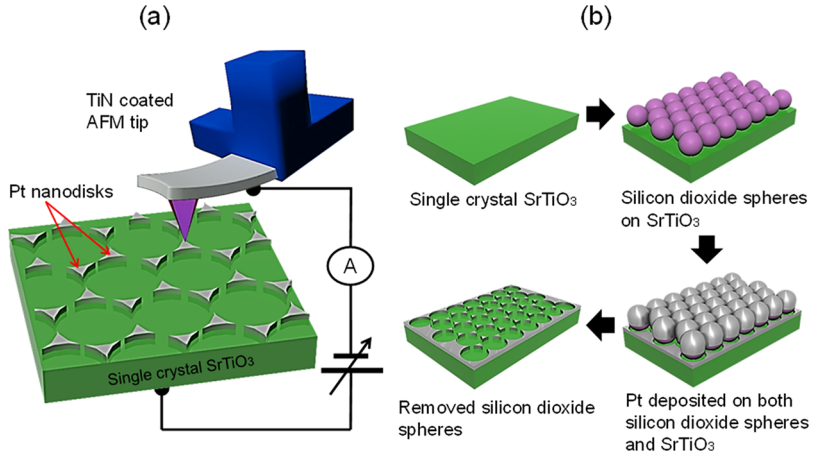


**Figure 1.** (a) Scheme for nanoscale bipolar RS phenomena on a triangular-shaped Pt nanodisks/Nb:STO single crystal Schottky junction; probing with conductive AFM at UHV. (b) Schemes of the experimental steps to fabricate triangular-shaped Pt nanodisks on a Nb:STO single crystal substrate.

Investigation of RS behaviors in a well-controlled environment is highly desirable.

Here, we investigated the bipolar RS phenomena of the nanoscale Pt/Nb:STO Schottky junction, prepared using the self-assembled nanopatterning method, in an ultrahigh vacuum (UHV) AFM system. We observed reproducible RS behavior of the randomly selected Pt/Nb:STO structure, which demonstrates competitive scaling and uniformity of RRAM devices composed of oxide Schottky junctions.

## 2. EXPERIMENTAL SECTION

**Materials and Methods.** Silica spheres were synthesized using the Stöber process[30] utilizing 10 mL of ethanol, 3.29 mL of distilled water, 0.55 mL of ammonium hydroxide ($NH_4OH$) (Daejung Chemicals, 25−28%), and 2.3 mL of tetraethylorthosilicate (TEOS) (Aldrich) at room temperature. The average size of the synthesized silica spheres was around 225 nm. The suspended products were prepared by diluting the silica spheres in 20 mL of methanol after rinsing four times with ethanol to obstruct aggregation of the silica spheres. A volume of 2 mL of the diluted silica sphere solution was used for monodispersion without drying. Sodium dodecyl sulfate (Aldrich) was added to the solution to acquire the hydrophilic−hydrophobic characteristics of the silica spheres, which improves the suspension of the silica spheres in the solution after ultrasonic dispersion for 30 min with heating. After adding 3 mL of chloroform, followed by sonication of the suspension for 60 min, 250 $\mu$L of the silica suspension was applied to the LB trough at an initial water surface area of 300 $cm^2$. We waited about 20 min to attain stabilization of the initial surface pressure before the isotherm process. The silica sphere monolayer was compressed using a barrier speed of 20 $cm^2$/min on the water surface with up to 11 mN/m for the target surface pressure. The monolayer of hexagonal close-packed (hcp) silica spheres was transferred to a $SrTiO_3$ (001) single crystal substrate, which was doped with Nb at 0.05 wt % (CrysTec, GmbH, Germany) by lifting up the vertical substrate at a velocity of 1 mm/min. The transfer ratio was about 1.

The ∼10 nm thick Pt electrode was deposited on both the hcp silica spheres and the remaining surface of the Nb:STO using e-beam evaporation. Afterward, we performed a 5 min ultrasonic treatment in ethanol and distilled water to remove the silica sphere monolayer because the silica spheres have a weaker bond strength with the $SrTiO_3$ substrate than the Pt metal. The resulting triangle-shaped Pt occur in the empty region between the absent silica spheres, as shown in Figure 1b.

**Characterization.** The morphology and conductance of the Pt nanodisks/Nb:STO single crystal were characterized using a titanium nitride (TiN) coated AFM tip (NT-MDT) with a cantilever force constant of 1.7 ± 0.2 N/m using UHV AFM (chamber with a base pressure of $1.0 \times 10^{-10}$ Torr; STM/AFM system, RHK-Technology) and ambient pressure AFM (5500, Agilent).[31,32] The current−voltage curves were obtained using point spectroscopy mode by applying an ±8 V sample bias. In addition, silver paste and indium were employed to make ohmic contact between the Nb:STO single crystal and the bottom metal plate, as shown in Figure 1a.

## 3. RESULTS AND DISCUSSION

Colloidal self-assembly combined with e-beam evaporation can be utilized to obtain nanoscale patterns of functional materials on the substrate with thermodynamically stable, two-dimensional (2D) hcp colloidal crystals as patterning masks.[33,34] To apply this process to the fabrication of nanoscale Pt/Nb:STO single crystal Schottky junctions, adequate self-assembly of a monolayer dispersed with colloidal crystals is required. The Langmuir−Blodgett (LB) technique can be utilized to acquire well-organized colloidal crystals with functionalized silicon dioxide spheres.[33,35] Therefore, we constructed hexagonal ordered triangular arrays, at the tens-of-nanometers scale, of Pt nanodisks on a Nb:STO single crystal substrate using a LB trough for colloidal lithography, as shown Figure 2a. This topographical image of unconnected 2D hcp Pt nanodisks on a Nb:STO single crystal was obtained using noncontact mode AFM at ambient pressure. The cross profile along the solid red

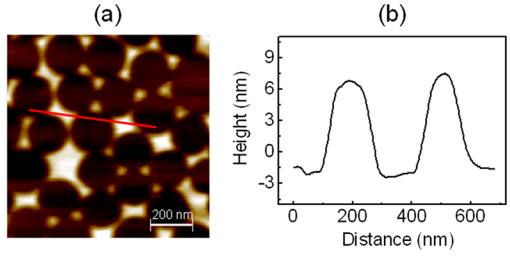


**Figure 2.** (a) Topographical image ($1.0 \times 1.0$ $\mu m^2$) of well-oriented Pt nanodisks/Nb:STO single crystal taken using noncontact mode AFM at ambient pressure with the fast scan direction along the *x*-axis. The bright and dark portions indicate the deposited Pt nanodisks and the surface of the Nb:STO single crystal, respectively. (b) The average height of the Pt nanodisk structures is ∼10 nm in the line profile along the red solid line in the topographical image.


dx.doi.org/10.1021/am4032086 | ACS Appl. Mater. Interfaces 2013, 5, 11668−11672

line in the topographical image shows ≤10 nm as the average height of the Pt nanodisks on Nb:STO, as shown Figure 2b.

Figure 3b shows representative reversible RS behavior when employing an n-type semiconductor as the switching cell

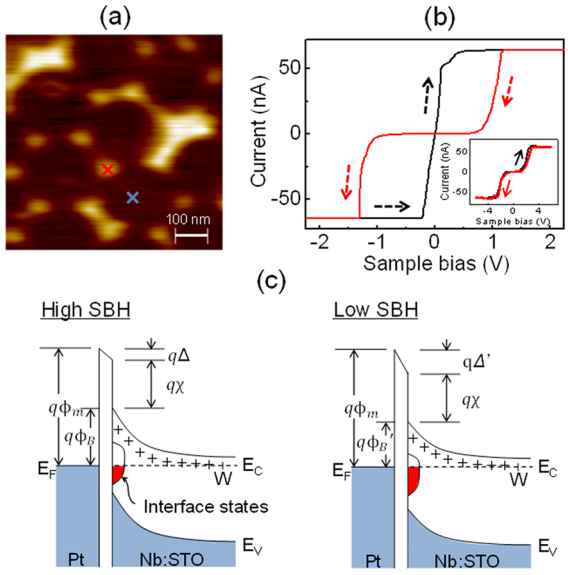


**Figure 3.** (a) Topographical image (700 × 700 nm$^2$) of hcp triangle-shaped Pt on a Nb:STO single crystal substrate obtained via contact mode AFM in UHV. (b) Bistable RS behavior was obtained on the Pt nanodisk marked with a red cross. The black and red dotted arrows represent the sweep direction from negative bias to positive bias and the reverse direction, respectively. Inset: $I-V$ curve measured at the $SrTiO_3$ surface with a ±8 V sweep bias. (c) Energy band diagrams of the Pt/Nb:STO junction showing high and low SBH along the applied potential and the charge and discharge of electrons at the interface states.

material on the triangular Pt nanodisk/Nb:STO (marked with a red cross in the topographical image in Figure 3a) by utilizing current−voltage spectroscopy at UHV around $10^{-10}$ Torr. The bistable RS sweep was taken using a sample bias of ±8 V on a Pt nanodisk ∼30 nm in lateral size. The inserted $I-V$ curve was obtained by direct contact on the $SrTiO_3$ substrate (marked with a blue cross in Figure 3a) using a TiN-coated metallic AFM tip, which did not show the hysteretic switching behavior. In Figure 3c, the energy band diagram of the Pt/Nb:STO junction shows the state of high ($\phi_B$) and low ($\phi_B'$) Schottky barrier height (SBH) according to the polarity of the external bias. Typically, the SBH in metal−semiconductor junctions is given by $\phi_B = \phi_m - \Delta - \chi$, where $\phi_m$ is the work function of Pt, Δ is the potential drop across the interface layer, and $\chi$ is the electron affinity of Nb:STO. The trapped charges are shown by the red area in Figure 3c. When the reverse bias voltage (a negative bias to Pt) is applied to the Schottky junction, the electrons and oxygen ions are repelled from the interface states to the bulk Nb:STO and high SBH is generally induced, which leads to switching from low-resistance state (LRS) to high-resistance state (HRS). Switching from HRS to LRS occurs in the forward bias voltage (a positive bias to Pt) region; accordingly, the electrons are charged in interface states that induce electron tunneling through the low-height Schottky barrier.[36] The polarity dependence of the RS behavior agrees with the model that is dominated by electron charge/discharge at interfacial trapping states.[2,37] The opposite polarity dependence of the RS behavior can be induced by migration of oxygen vacancies.[21] Redox at the $SrTiO_3$ surface is difficult at UHV and cannot be a plausible scenario for the reversible RS phenomena in our experiment. The extrinsic effects (e.g., structural defects and off stoichiometry, which are unavoidable in thin films) cannot be regarded as major factors influencing the RS behavior of our single-crystalline sample.[22]

Figure 4a shows a topographical image of the Pt nanodisks on a Nb:STO single crystal, which consists of both partially

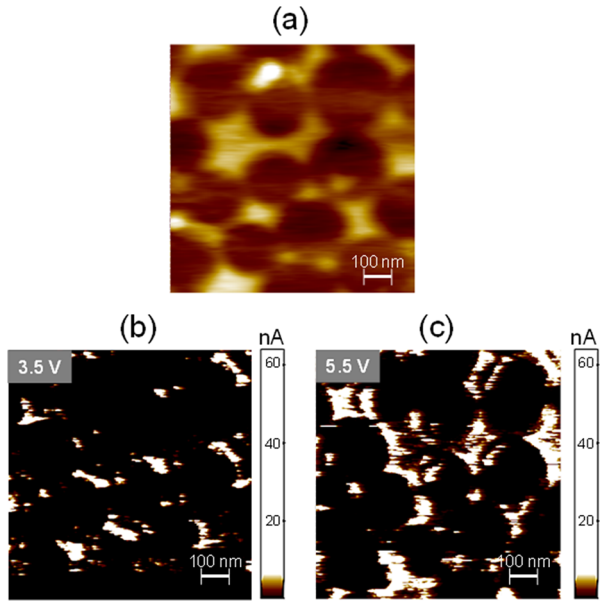


**Figure 4.** Conductive AFM images of Pt nanodisks on a Nb:STO single crystal when various sample bias voltages were applied to the Schottky junction. (a) The topographical image (1.0 × 1.0 $\mu$m$^2$) was obtained on a corresponding region with spatial mapping of the current. (b,c) Conductance images where the bright regions indicate a higher current flow than the dark regions. The sample bias voltage was changed by (b) 3.5 V and (c) 5.5 V. The applied load during the measurements was 8.5 nN.

connected and nonconnected Pt metal disks. When an external bias of 3.5 V was applied to the sample, the current signal particularly appeared at the boundary of the Pt nanodisks, as shown Figure 4b. As the sample bias voltage increased, most of the Pt nanodisks show a large current signal at both the boundary and inside the Pt nanodisks under 5.5 V of sample bias (Figure 4c). The current images show a higher conductance at the Pt nanodisks/Nb:STO than that on the Nb:STO because the Pt nanodisks occupy a larger contact area as the top electrode than the AFM tip on the Nb:STO substrate. Furthermore, higher conductance along the boundary of the Pt nanodisks, such as the morphological inhomogeneity in the spatial current mapping, is generally observed due to the larger contact area between the metallic AFM tip and the sample.[15]

The reproducible RS behavior of the well-organized individual conducting dots in the epitaxial $SrTiO_3$ thin film was reported using conductive AFM with a metallic probe.[22] Although such experiments report nanoscale switching, control of the switching location is impossible when utilizing dislocations or defects in the thin films as the preferential migration path of the oxygen vacancies. Thus, observation of the nanoscale RS process in thin films cannot guarantee successful scaling down of the RRAM device. In contrast, our

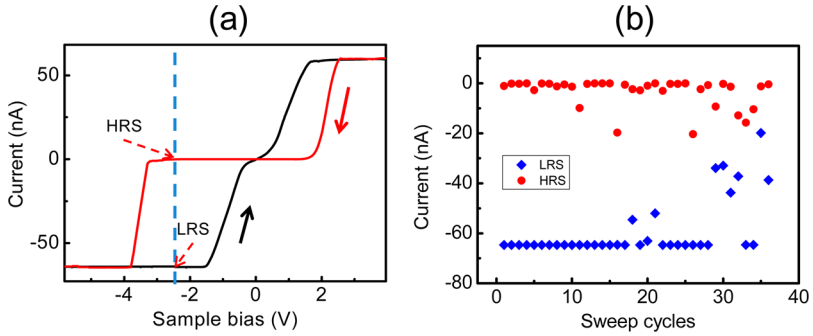


**Figure 5.** Current−voltage spectroscopy was continually performed on the Pt nanodisk/Nb:STO single crystal for 36 dc sweep cycles to examine endurance. (a) Representative RS behavior shows that both HRS and LRS were obtained at the −2.5 V sample bias voltage in the sweep curves. A sweep speed of 2.01 V/s was employed. The applied load during the measurement was 8.5 nN. (b) The endurance behavior was shown in the distributed negative current region.

experiment clearly demonstrates RS behaviors in the nanoscale Schottky junction fabricated at the desired location.

The near-surface electrochemical redox reaction, one of the primary scenarios in RS, has attracted considerable attention. In a few reports, the charge transfer reaction, incorporating oxygen ions into the surface of NiO, was much more dominant than the migration of decomposed oxygen ions within the NiO film for RS phenomena at ambient conditions.[25] In addition, the surface potential of $TiO_2$ can be determined by reduction of the ambient state in a partial vapor pressure of $H_2$/Ar and the amount of $O_2$ adsorption.[26] Both oxygen vacancy formation in the transition metal−oxide film and incorporation of the charge carrier have been considered major RS mechanisms at ambient pressure.[21−23,25] In contrast, such scenarios based on oxygen vacancy generation and migration do not explain the RS behaviors of our Pt/Nb:STO Schottky junctions. First, the switching polarity has the opposite trend as the direction of vacancy migration. Second, there is no oxygen reservoir to resupply the oxygen ions to the sample under UHV. However, we may not completely ignore the importance of oxygen vacancies in our Nb:STO sample. Migration of oxygen vacancies should result in the creation of defect states, which act as trapping states for the carriers. Therefore, the drift and diffusion of oxygen vacancies can play a crucial role in the RS mechanism in our Schottky junctions.

It is important to investigate the durability of the RS phenomena in metal/semiconductor Schottky junctions. Figure 5a shows where the measurements were taken (sample bias of −2.5 V) in the repeated current−voltage curve of the Pt nanodisk/Nb:STO in the reverse bias territory. The retention time of the resistance states was generally estimated to be $10^3$−$10^4$ s in the Pt/$SrTiO_3$ junction.[38] The current distribution for LRS and HRS on the Pt nanodisk/Nb:STO single crystal during 36 dc sweep cycles is shown in Figure 5b. This endurance characteristic was measured on one Pt nanodisk without moving the AFM cantilever in the lateral direction. We employed a sweep sample bias voltage of ±8 V and sweep rate of 2.01 V/s, which were generally utilized for observation of the bipolar RS behavior. The difference of current level between LRS and HRS was approximately 64 nA due to the current being limited by the output of the current−voltage converter. The scattered points after 30 dc sweep cycles occurred mainly due to drift of the AFM probe, which prefers to remain perpendicular to the sample surface because it is difficult for the piezo actuator, which controls the three-dimentional movement of the AFM scanner, to remain at a fixed point for a long time even though a constant bias voltage is applied. The horizontal drift of the piezo actuator with movement of the *X*- and *Y*-axis in the AFM scanner was 0.6 nm/s. The lateral size of Pt nanodisk used to measure the durability of the RS phenomena was approximately 150 nm. Additionally, vertical drift of the Z scanner as well as instability of the electrical contact between the tip and sample during *I*−*V* measurement could be responsible for failure of the switching behavior. Such difficulties in the actual measurement, rather than the intrinsic RS mechanism in our junctions, may limit the number of repeated switching cycles. The results suggest that the Schottky-type RS device can be scaled down to the 10 nm range and realized at a controlled position for high-density RRAM devices.

## 4. CONCLUSIONS

The reproducible RS behaviors of Pt and single-crystalline Nb:STO Schottky contacts at the nanometer scale were demonstrated with conductive AFM under UHV. Bipolar RS behaviors of a triangular-shaped Pt/Nb:STO single crystal junction, based on the interfacial charge trapping/detrapping mechanism, were acquired by utilizing local current−voltage spectroscopy. The resistance states (either HRS or LRS) of a specific Schottky contact during voltage sweeping could be identified by spatial mapping of the conductance, which was obtained simultaneously via topographical images. The bipolar RS behavior of 10 nm Pt/Nb:STO Schottky junctions can be repeated for 36 dc sweep cycles.

## AUTHOR INFORMATION

### Corresponding Authors

*E-mail: dwkim@ewha.ac.kr (D.-W.K.).
*E-mail: jeongypark@kaist.ac.kr (J.Y.P.).

### Notes

The authors declare no competing financial interest.

## ACKNOWLEDGMENTS

This work was supported by 2012R1A2A1A01009249 through the National Research Foundation and the Research Center Program (CA1201) of IBS (Institute for Basic Science), Republic of Korea.

## REFERENCES

(1) Chang, S. H.; Lee, J. S.; Chae, S. C.; Lee, S. B.; Liu, C.; Kahng, B.; Kim, D. W.; Noh, T. W. *Phys. Rev. Lett.* **2009**, *102*, 026801.

(2) Fujii, T.; Kawasaki, M.; Sawa, A.; Kawazoe, Y.; Akoh, H.; Tokura, Y. *Phys. Rev. B* **2007**, *75*, 165101.
(3) Kwon, D. H.; Kim, K. M.; Jang, J. H.; Jeon, J. M.; Lee, M. H.; Kim, G. H.; Li, X. S.; Park, G. S.; Lee, B.; Han, S.; Kim, M.; Hwang, C. S. *Nat. Nanotechnol.* **2010**, *5*, 148−153.
(4) Park, C.; Seo, Y.; Jung, J.; Kim, D. W. *J. Appl. Phys.* **2008**, *103*, 054106.
(5) Shima, H.; Zhong, N.; Akinaga, H. *Appl. Phys. Lett.* **2009**, *94*, 082905.
(6) Tamura, T.; Ishibashi, S.; Terakura, K.; Weng, H. M. *Phys. Rev. B* **2009**, *80*, 195302.
(7) Waser, R.; Aono, M. *Nat. Mater.* **2007**, *6*, 833−840.
(8) Waser, R.; Dittmann, R.; Staikov, G.; Szot, K. *Adv. Mater.* **2009**, *21*, 2632−2663.
(9) Yang, J. J.; Pickett, M. D.; Li, X. M.; Ohlberg, D. A. A.; Stewart, D. R.; Williams, R. S. *Nat. Nanotechnol.* **2008**, *3*, 429−433.
(10) Strukov, D. B.; Snider, G. S.; Stewart, D. R.; Williams, R. S. *Nature* **2008**, *453*, 80−83.
(11) Yang, J. J.; Strukov, D. B.; Stewart, D. R. *Nat. Nanotechnol.* **2013**, *8*, 13−24.
(12) Chang, S. H.; Lee, S. B.; Jeon, D. Y.; Park, S. J.; Kim, G. T.; Yang, S. M.; Chae, S. C.; Yoo, H. K.; Kang, B. S.; Lee, M. J.; Noh, T. W. *Adv. Mater.* **2011**, *23*, 4063−4067.
(13) Shin, J.; Kim, I.; Biju, K. P.; Jo, M.; Park, J.; Lee, J.; Jung, S.; Lee, W.; Kim, S.; Park, S.; Hwang, H. *J. Appl. Phys.* **2011**, *109*, 033712.
(14) Kim, G. H.; Lee, J. H.; Jeon, W.; Seok, J. Y.; Yoon, J. H.; Yoon, K. J.; Park, T. J.; Hwang, C. S. *ACS Appl. Mater. Interfaces* **2012**, *4*, 5338−5345.
(15) Lee, M. H.; Hwang, C. S. *Nanoscale* **2011**, *3*, 490−502.
(16) Kwon, S.; Seo, H.; Lee, H.; Jeon, K. J.; Park, J. Y. *Appl. Phys. Lett.* **2012**, *100*, 123101.
(17) Park, J. Y.; Maier, S.; Hendriksen, B.; Salmeron, M. *Mater. Today* **2010**, *13*, 38−45.
(18) Yoon, J. H.; Han, J. H.; Jung, J. S.; Jeon, W.; Kim, G. H.; Song, S. J.; Seok, J. Y.; Yoon, K. J.; Lee, M. H.; Hwang, C. S. *Adv. Mater.* **2013**, *25*, 1987−1992.
(19) Alexe, M.; Gruverman, A.; Harnagea, C.; Zakharov, N. D.; Pignolet, A.; Hesse, D.; Scott, J. F. *Appl. Phys. Lett.* **1999**, *75*, 1158−1160.
(20) Alexe, M.; Harnagea, C.; Hesse, D.; Gosele, U. *Appl. Phys. Lett.* **1999**, *75*, 1793−1795.
(21) Szot, K.; Speier, W.; Bihlmayer, G.; Waser, R. *Nat. Mater.* **2006**, *5*, 312−320.
(22) Szot, K.; Dittmann, R.; Speier, W.; Waser, R. *Phys. Status Solidi RRL* **2007**, *1*, R86−R88.
(23) Muenstermann, R.; Dittmann, R.; Szot, K.; Mi, S. B.; Jia, C. L.; Meuffels, P.; Waser, R. *Appl. Phys. Lett.* **2008**, *93*, 023110.
(24) Muenstermann, R.; Menke, T.; Dittmann, R.; Waser, R. *Adv. Mater.* **2010**, *22*, 4819−4822.
(25) Lee, M. H.; Song, S. J.; Kim, K. M.; Kim, G. H.; Seok, J. Y.; Yoon, J. H.; Hwang, C. S. *Appl. Phys. Lett.* **2010**, *97*, 062909.
(26) Kim, H.; Hong, S.; Kim, D. W. *Appl. Phys. Lett.* **2012**, *100*, 022901.
(27) Oshea, S. J.; Atta, R. M.; Welland, M. E. *Rev. Sci. Instrum.* **1995**, *66*, 2508−2512.
(28) Peter, F.; Szot, K.; Waser, R.; Reichenberg, B.; Tiedke, S.; Szade, J. *Appl. Phys. Lett.* **2004**, *85*, 2896−2898.
(29) Burnham, N. A.; Colton, R. J.; Pollock, H. M. *J. Vac. Sci. Technol., A* **1991**, *9*, 2548−2556.
(30) Stöber, W.; Fink, A. *J. Colloid Interface Sci.* **1968**, *26*, 62−69.
(31) Kwon, S.; Choi, S.; Chung, H. J.; Yang, H.; Seo, S.; Jhi, S. H.; Park, J. Y. *Appl. Phys. Lett.* **2011**, *99*, 013110.
(32) Park, J. Y.; Qi, Y. B. *Scanning* **2010**, *32*, 257−264.
(33) Van, T. N.; Lee, Y. K.; Lee, J.; Park, J. Y. *Langmuir* **2013**, *29*, 3054−3060.
(34) Zhang, J. H.; Li, Y. F.; Zhang, X. M.; Yang, B. *Adv. Mater.* **2010**, *22*, 4249−4269.
(35) Reculusa, S.; Ravaine, S. *Chem. Mater.* **2003**, *15*, 598−605.
(36) Zou, X.; Ong, H. G.; You, L.; Chen, W. G.; Ding, H.; Funakubo, H.; Chen, L.; Wang, J. L. *AIP Adv.* **2012**, *2*, 032166.
(37) Bourim, E. M.; Kim, D. W. *Curr. Appl. Phys.* **2013**, *13*, 505−509.
(38) Gwon, M.; Lee, E.; Sohn, A.; Bourim, E.; Kim, D. W. *J. Korean Phys. Soc.* **2010**, *57*, 1432−1436.